ACS OMEGA

http://pubs.acs.org/journal/acsodf

Article

Molecularly Engineered Surfactin Analogues Induce Nonapoptotic-Like Cell Death and Increased Selectivity in Multiple Breast Cancer Cell Types

Rebecca T. Miceli, Filbert Totsingan, Tasnim Naina, Samita Islam, Jonathan S. Dordick, David T. Corr, and Richard A. Gross*

Cite This: *ACS Omega* 2023, 8, 14610−14620

Read Online

ACCESS | Metrics & More | Article Recommendations | Supporting Information

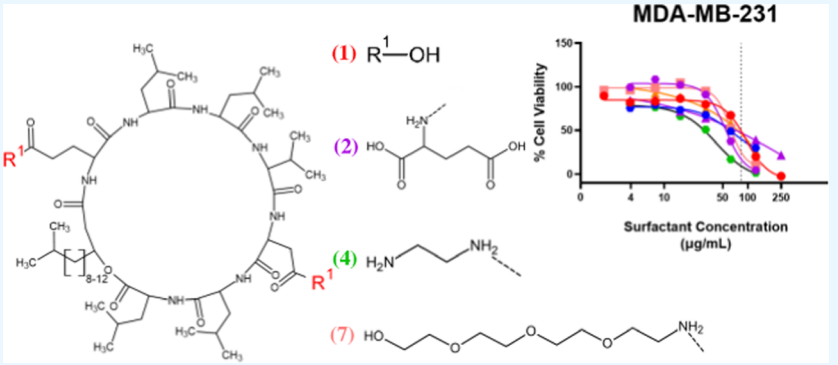

ABSTRACT: Surfactin, a negatively charged amphiphilic lipopeptide biosurfactant, is synthesized by the bacterium *Bacillus subtilis*. It consists of a cyclic heptapeptide and an 11−15C β-hydroxy fatty acid. To probe how the modification of the molecular skeleton of surfactin influences its selectivity and activity against breast cancer, six synthetic surfactins were generated. Modifications were accomplished by conjugating amine-functionalized molecules to the Glu and Asp carboxyl moieties of the heptapeptide. The resulting synthetic surfactins provided a diverse series of molecules with differences in charge, size, and hydrophilicity. After purification and structural analysis, insights into biological activity and specificity were generated for each compound. Dose-dependent growth inhibition was determined for four tumorigenic breast cancer cell lines in monolayer and spheroid morphologies, as well as nontumorigenic fibroblasts and sheep erythrocytes, which were utilized to determine selectivity indices. Results indicated that two compounds, which have amplified anionic charge, had increased activity on breast cancer, with reduced activity on nontumorigenic fibroblasts and erythrocytes. Cationic derivative surf-ethylenediamine has increased activity on all cell lines tested. Novel correlations between dose−response activities and physicochemical properties of all compounds determined that there is a significant correlation between the critical micelle concentration and activity against multiple cell lines.

Biosurfactants are amphiphilic molecules produced from bacteria and nonpathogenic yeasts, often reaching high fermentation titers and displaying anticancer, anti-inflammatory, antimicrobial, antifungal, and antiviral activities, making them promising low-cost therapeutic candidates to meet increasingly stringent sustainability metrics.[1−6] Surfactin, compound **1**, a negatively charged lipopeptide biosurfactant, is produced by Gram-positive endospore-forming *Bacillus subtilis* bacterial strains in yields of up to 26.5 g/L.[7−10] Surfactin (Scheme 1) is composed of the heptapeptide (L)-Glu−(L)-Leu−(L)-Leu−(L)-Val−(L)-Asp−(D)-Leu−(L)-Leu, cyclized by an 11-to-15 carbon chain length β-hydroxy fatty acid that forms an amide with the α-amino group of (L)-Glu and an ester group with the α-carboxyl moiety of (L)-Leu.[11] The amphiphilic character of surfactin is due to the dual presence of hydrophilic and negatively charged (L)-Glu and (L)-Asp residues, as well as hydrophobic amino acids and a fatty acid moiety. Surfactin presents valuable therapeutic characteristics including anticancer and anti-inflammatory activities.[12]

Breast cancer is diagnosed approximately 1.7 million times per year around the globe, with nearly one-half of these diagnoses, and 62% of yearly breast cancer mortalities occur in developing countries.[13] Consequently, low-cost, selective drug alternatives for the treatment of breast cancers are desperately

Received: January 22, 2023
Accepted: March 1, 2023
Published: April 10, 2023

Scheme 1. Structures of Surfactin and Its Synthetic Analogues Characterized in This Paper. Surfactin (1) and Its Synthetic Derivatives. Anionic Derivatives: Surf-Glutamic Acid (2) and Surf-Aspartic Acid (3); Cationic Derivatives: Surf-Ethylenediamine (4), Surf-Guanidine (5), and Surf-Histamine (6). Neutral Derivative: Surf-Tetraethylene Glycol Monoamine (7)

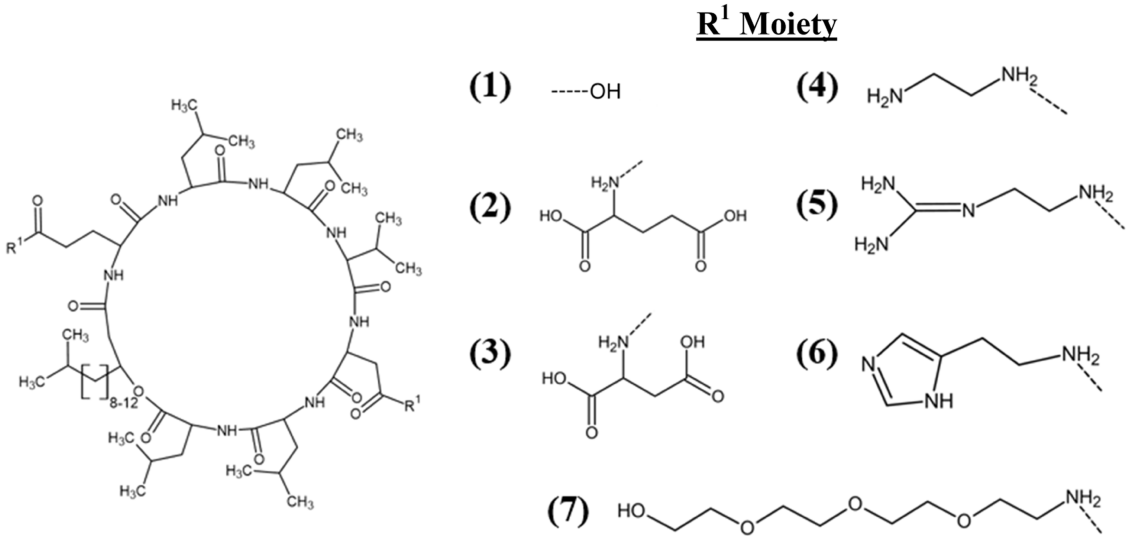

needed. Not only are current treatment options expensive but they typically rely on nontargeted chemotherapeutics such as doxorubicin or paclitaxel.[14] Surfactin has been reported to cause cell cycle arrest, antiproliferation, and apoptosis in human colon carcinoma,[15] human breast cancer,[16,17] ovarian cancer,[18] and osteosarcoma.[19] Surfactin is selective for tumorigenic over nontumorigenic cell lines when treated at an established therapeutic IC_{50}, including 100% cell viability for nontumorigenic keratinocytes (30 μM) compared against oral squamous cells[20] and osteoblasts (5 μM) compared against osteosarcoma.[19] Unfortunately, surfactin has high hemolytic activity. In one example, the rapid lysis of erythrocytes occurred at 40 μM, the therapeutic dose used for viral inactivation.[21]

An important pursuit in drug development is through investigations that map out structure−activity relationships (SARs) to optimize a drug candidate's therapeutic efficacy. However, for surfactin, little is known about how structural modifications can lead to beneficial changes in its therapeutic potential as an anticancer drug. Nonetheless, there is some literature that can guide us in developing a surfactin SAR against cancer cell lines. Surfactin analogues differing in β-hydroxyl fatty acid chain lengths have been isolated. Subsequent studies revealed that the C_{15} β-hydroxyl fatty acid chain length had the strongest inactivation activity against a variety of cancer cells.[20−23] Additionally, conversion of the Glu-γ and Asp-β carboxylic acids of the heptapeptide into the corresponding methyl ester derivative resulted in an increased IC_{50} toward HeLa cells, from 25.2 μg/mL for C_{15}-surfactin to 47.7 μg/mL for the C_{15}-surfactin-O-methyl ester derivative. This indicates that the amphiphilic character of surfactin is important to its inhibitory activity.[22] Synthetic linear surfactin analogues have been chemically synthesized that exhibited improved selectivity toward porcine epidemic diarrhea virus over erythrocytes, improving a selectivity index from 4 for surfactin to 82 for the linear compound SLP8.[24]

Herein, we exploit the availability of reactive free carboxyl side chains of surfactin Asp and Glu moieties as sites to conjugate amines to form stable amide derivatives (Scheme 1). The amines were selected to introduce major changes in surfactin physicochemical characteristics such as charge (e.g., cationic, anionic, and neutral derivatives), critical micelle concentration (CMC), hydrophilic−lipophilic balance (HLB), hydrogen bond donors/acceptors, permeability constants ($c\log P$, $\log D$), pK_a, and charge at a given pH. Structural analysis of the synthesized surfactin analogues was performed by nuclear magnetic resonance (NMR) spectroscopy and liquid chromatography-mass spectrometry (LC-MS). SAR relationships were established by determining the biological activity, defined as the cytotoxicity caused by the action of surfactin and its synthetic analogues on the specified cell type. Activities are reported as half-maximal inhibitory concentration (IC_{50}), defined by the concentration at which cell growth is inhibited by 50%. In this paper, we dosed two-dimensional monolayers of the breast cancer cell lines MDA-MB-231, AU565, BT-474, and MCF-7. Values of the selectivity indices (SIs) were determined by dosing sheep erythrocytes and nontumorigenic human dermal fibroblast cell line, CCD1065SK HDF, with the surfactin analogues. In addition to traditional monolayer studies, IC_{50} values were determined using three-dimensional spheroid cell models that better mimic the pathophysiologic gradients and cell−cell and cell−matrix interactions observed *in vivo*, leading to higher IC_{50} values.[25−27] Comparison of the modified surfactin analogues revealed structural changes that both increased activity on breast cancer cell lines and caused large reductions in surfactin hemolytic activity, thus improving the SI for several of the synthetic surfactin analogues. As a result, six novel surfactin derivatives, compounds **2**−**7**, were prepared and characterized and may provide a low-cost chemotherapeutic option to treat patients worldwide.

RESULTS AND DISCUSSION

Synthesis and Characterization of Synthetic Surfactin Analogues. Compound **1** was amidated at the carboxyl side chains of L-Glu and L-Asp moieties by conjugating the following amines: L-Glu(t-Bu)$_2$ (**2**), L-Asp(t-Bu)$_2$ (**3**), N-Boc-ethylenediamine (**4**), 2-(2-aminoethyl)-1,3-diBOC guanidine

https://doi.org/10.1021/acsomega.3c00454
ACS Omega 2023, 8, 14610−14620

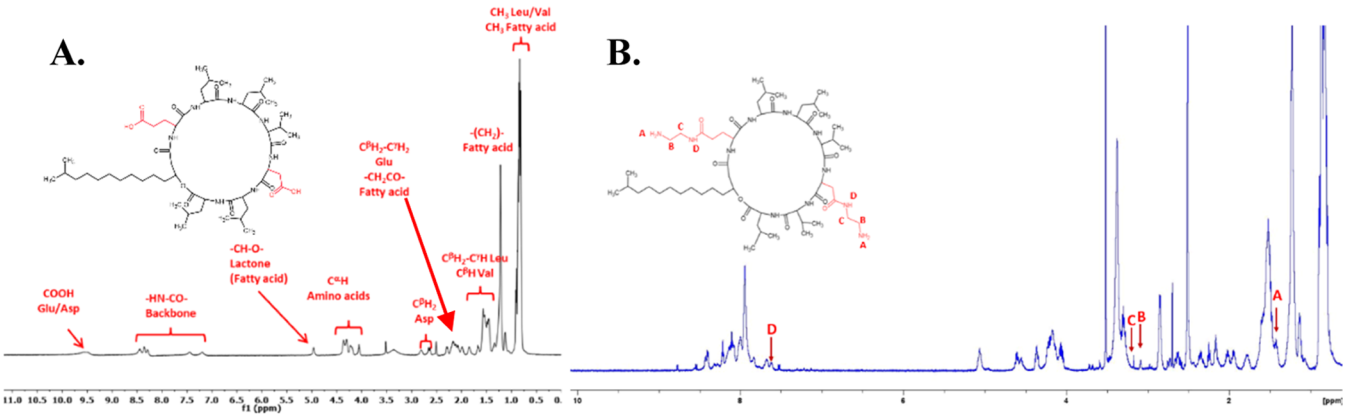

Figure 1. Proton (^{1}H) NMR spectra (600 MHz, DMSO-d_6) of **1** (A) and **2** (B). Protons that correlate with amide-modified moieties are marked in red. They consist of NMR resonances with peaks at 1.8, 3.2, 3.3, and 7.6 ppm that are assigned to the NH_2, two methylene (CH_2), and NH protons of the ethylenediamine moiety, respectively. NMR captured using a 600 MHz Bruker NMR in DMSO-d6. Analysis of all analogues in Figures S3–S15.

Table 1. Structural and Physicochemical Characteristics of Compounds 1–7

compound	[a]MW (Da)	[b]HBD	[c]HBA	[d]*c* log *P*	CMC (μg/mL)	[e]HLB	pK_a acid	[f]log *D* pH 7.4	charge at pH 7.4
1	1036	9.0	12	6.2	9.5	29.6	3.8	0.0	−2.0
2	1294	13	18	4.0	43.7	52.7	2.9	−7.4	−4.0
3	1266	13	18	4.5	18.5	52.1	3.7	−6.7	−4.0
4	1106	11	12	3.1	3.1	59.1	11.6	−0.4	1.9
5	1208	15	16	1.6	14.7	59.3	11.6	−2.4	2.0
6	1190	11	12	4.5	8.9	46.9	11.4	4.5	0.3
7	1386	11	18	3.4	3.4	51.7	11.5	3.4	0.0

[a]Molecular weight (MW). [b]Hydrogen bond donor (HBD). [c]Hydrogen bond acceptor (HBA). [d]Calculated partition coefficient (*c* Log *P*). [e]Hydrophilic–lipophilic balance (HLB). [f]Distribution coefficient at pH 7.4 (log *D*). Values were generated with the Chemicalize Software package, excluding CMC, which was determined experimentally.

(**5**), L-histamine (**6**), and tetraethylene glycol monoamine (**7**). Structural characterization was performed by 1D and ^{1}H–^{1}H correlation spectroscopy (COSY), ^{1}H NMR spectroscopy, and LC-MS (Figures S1–S3). As an example, Figure 1 displays the comparison between ^{1}H NMR spectra of **1** and **4** derivatives. The spectrum of **4** showed characteristic peaks consistent with the structure of **1**. Additional peaks at 1.8, 3.2, 3.3, and 7.6 ppm were assigned to the NH_2, two methylene (CH_2), and NH protons of the ethylenediamine moiety, respectively. Confirmation of these assignments was based on a ^{1}H–^{1}H COSY spectrum. Furthermore, LC-MS had peaks at m/z = 1092, 1106, and 1120 [M + H$^+$], consistent with the expected value of 1106 ± 14, which represents a C13 ± CH_2 β-hydroxy fatty acid chain lengths. Other **1** analogues exhibited ^{1}H NMR signals and LC-MS data consistent with their structures. Corresponding data and spectra are displayed in Figures S4–S15.

Structural information on **1** and its analogues was generated both experimentally and with Chemicalize software to calculate values specified within the Lipinski rule of 5 for orally bioavailable drugs (Table 1).[28] These values include charge at pH 7.4, molecular weight (MW), number of hydrogen bond donor groups (HBD), number of hydrogen bond acceptor groups (HBA), calculated partition coefficient (*c* log *P*), hydrophilic–lipophilic balance (HLB), and distribution coefficient at pH 7.4 (log *D*). Experimentally determined critical micelle concentration (CMC) values of natural and synthetic surfactin analogues were determined as described in the Materials and Experimental Methods section. Plots of surface tension *vs* surfactant concentration are displayed in Figure S16. The CMC of **1** is 9.5 μg/mL, consistent with a previous report.[29] Analogues **2** and **3**, which present four carboxylic acid groups, have CMC values of 43.7 and 18.5 μg/mL, respectively. Hence, increasing the density of carboxylic groups relative to **1** resulted in a lower propensity of the analogues to organize at the air–water interface, likely due to higher water solubility and charge–charge repulsion. The CMC of positively charged **3** and neutrally charged **7** are nearly threefold lower than that of **1**. Chemicalize software generated *c* log *P* values for each analogue. A high *c* log *P* value correlates with a high degree of hydrophobicity. Surfactin is more hydrophobic than all of the synthesized analogues, which have *c* log *P* values ≤ 5, thereby suggesting that the analogues are likely not appropriate for oral administration.[28]

Biological Activity of Surfactin and Its Synthetic Analogues in 2D Cultures. Four breast cancer cell lines, differing in aggressiveness, morphology, and specific cell receptor (HR, hormone receptor; ER, estrogen receptor, PR, progesterone receptor), were selected for determination for dose–response studies for each surfactin analogue shown in Figure 2. The BT-474 cells (ER, PR, and HER2 positive) and MCF-7 cells (ER and PR positive) are typically easier to treat and are much less aggressive than the AU565 (HER2 overexpressing) and MDA-MB-231 (ER, PR, and HER2 negative) breast cancer cell lines.[30] SI values were calculated from IC_{50} values determined for nontumorigenic CCD1065SK breast-derived fibroblast (HDF) and erythrocyte toxicity using sheep red blood cells.

Traditional 2D monolayer cultures were used to assess the activity of **1** and its analogues against tumorigenic and

https://doi.org/10.1021/acsomega.3c00454
ACS Omega 2023, 8, 14610–14620

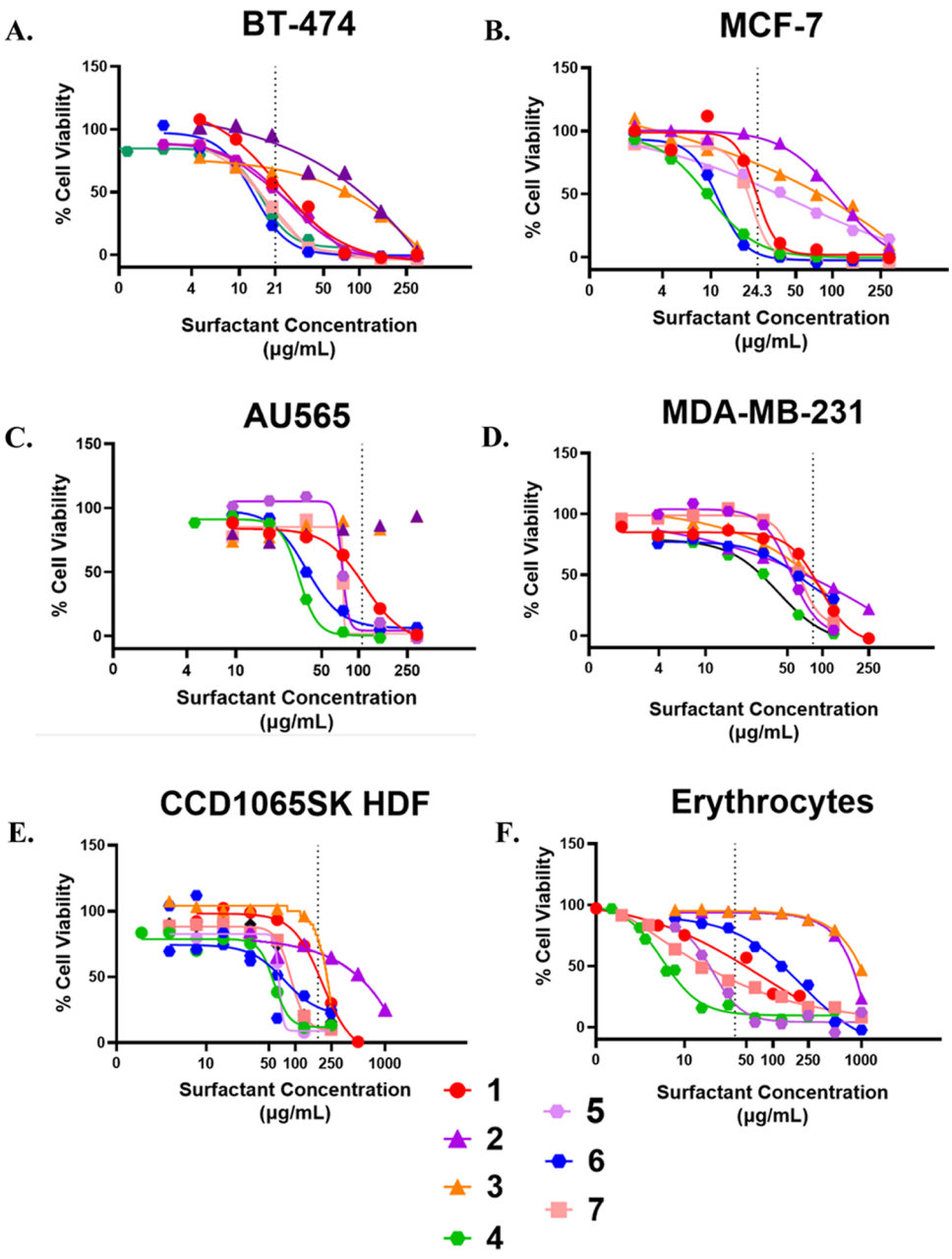

Figure 2. Dose−response curves of surfactin and synthetic analogues after 24 h of treatment on tumorigenic and nontumorigenic cell lines. BT-474 (A), MCF-7 (B), AU565 (C), MDA-MB-231 (D), CCD1065SK HDF (E), and erythrocytes (F). All experiments were performed in triplicate. IC_{50} determined with AbsoluteIC50 nonlinear regression curve on GraphPad Prism9. IC_{50} values are shown in Table 2. The dotted vertical line represents the IC_{50} of **1**.

Table 2. IC_{50} Values for 2D Monolayers of Six Cell Lines[a,b]

compound	BT-474	MCF-7	AU565	MDA-MB-231	CCD1065SK HDF	erythrocytes
1	21	24	110	84	180	38
2	85	56	>300	58	380	760
3	110	44	>300	46	210	1160
4	16	10	32	32	97	6.9
5	24	27	74	53	80	23
6	13	11	39	60	31	120
7	16	21	75	64	90	11

[a]Dose−response curves are provided in Figure 2 for compounds **1**−**7**. [b]Note: values represented as μg/mL, n = 3/dose.

nontumorigenic cell lines. Following a 24 h treatment of **1**, dose-dependent cell viability was studied and IC_{50} values (Table 2) were calculated against the aforementioned four breast cancer cell lines (Figure 2). Compound **1** was fivefold

https://doi.org/10.1021/acsomega.3c00454
ACS Omega 2023, 8, 14610−14620

more cytotoxic toward the BT-474 (21 μg/mL) and MCF-7 (24 μg/mL) cell lines, compared with the AU565 (110 μg/mL) and MDA-MB-231 (84 μg/mL) cell lines. Against nontumorigenic human dermal fibroblasts, CCD1065SK, **1** had an IC_{50} of 180 μg/mL. A relatively low IC_{50} (38 μg/mL) was measured when dosing sheep erythrocytes with **1**, confirming the relatively high hemolytic activity of surfactin.[21,31,32] The objective herein was to improve surfactin's activity and selectivity against breast cancer through selective amidation of Asp and Glu moieties on the surfactin heptapeptide.

Identical treatment conditions to that of **1** were employed to determine corresponding IC_{50} values for each of the six synthetically produced surfactin analogues (Figure 2). Compounds **2** and **3** had double the anionic charge than **1** and both had moderate IC_{50} values against all breast cancer cell lines, ranging from 44 to 110 μg/mL, except for AU565 cells (>300 μg/mL). Hence, amplification of the negative charge at surfactin Asp and Glu sites substantially lowered its activity against the AU565 line. However, amplification of the negative charge reduced activity against nontumorigenic cell lines CCD1065SK HDF (380 and 210 μg/mL, respectively) and sheep erythrocytes (1160 and 760 μg/mL, respectively) compared with **1**, substantially improving their respective SIs.

All three cationic derivatives improved or matched the corresponding IC_{50} value with **1** on the corresponding breast cancer cell lines. The largest improvement in the IC_{50} value was from **4**, which was the most cytotoxic compound against all four breast cancer cell lines, with IC_{50} values ranging from 10 μg/mL (MCF-7) to 32 μg/mL (AU565). This is likely due to the charged interactions between the cationic surfactin analogue and the negatively charged cancer cell lipid bilayer. Unfortunately, compound **4** also had increased activity on nontumorigenic CCD1065SK (97.3 μg/mL). The cationic derivative that was the most biologically active toward CCD1065SK was **6**, with an IC_{50} value of only 31 μg/mL. Compound **4** had increased activity against sheep erythrocytes (6.9 μg/mL), whereas **6** had a 3-fold higher IC_{50} on erythrocyte activity (120 μg/mL) compared with **1**. Compared to **1**, the neutral **7** had similar IC_{50} values against the breast cancer BT-474 (16 μg/mL) and MCF-7 (21 μg/mL) cell lines; however, the IC_{50} values were slightly increased against AU565 (75 μg/mL) and MDA-MB-231 (64 μg/mL) cell lines. Compound **7** also had a 2-fold increase in activity against CCD1065SK and a 4-fold increase in activity against erythrocytes (11 μg/mL) compared with **1**. Hence, neutral **7** appears to interact with the negatively charged cell lipid membranes present in these two cell lines.

Selectivity of Surfactin and Its Synthetic Analogues toward Cancer Cell Lines. Selectivity index is generated as a ratio of the lethal dose to the therapeutic dose of a given substance. The fibroblast and red blood cell IC_{50} values represent the lethal dose (LD_{50}), while the IC_{50} of a given drug is defined as the effective dose (ED_{50}).[33] An SI greater than or equal to 3 has been used as a criterion warranting continued studies of the candidate anticancer drug.[33] The corresponding SI values reveal that **2** (exception BT-474 cells), **3**, and **4** have SI's $\geq$ 3, while **5**, **6**, and **7** (exception MCF-7 and BT-474) fall below the SI threshold of 3 when compared against fibroblasts (Table 3). The highest SI values for MCF-7 and BT-474 cells, determined using the fibroblast cell line, were observed with **1** (7.4 and 8.5, respectively) and **4** (10.3 and 6.3, respectively). For AU565, SI values were all $\leq$ 3.0, whereas, for MDA-MB-231, the SI value for **3** reached 6.6. SI values calculated for red blood cells were largely increased by increasing the negative charge of surfactin molecules (Table 4). Specifically, **3** reached SI values of 25.5, 26.3, and 10.6 for the breast cancer cell lines MDA-MB-231, MCF-7, and BT-474, respectively. Similarly, **2** reached SI values of 13.0, 13.6, and 8.9, respectively. Other modifications that showed substantial increases in SI using red blood cell HD_{50} values are **6** for MCF-7 (11.2) and **7** for BT-474 (7.4).

Table 3. Selective Indices (SIs) of 1−7[a]

compound	BT-474	MCF-7	AU565	MDA-MB-231
1	8.6	7.5	1.6	2.1
2	4.5	6.8	N/A	6.6
3	1.9	4.8	N/A	4.6
4	6.1	9.7	3.0	3.0
5	3.3	3.0	1.1	1.5
6	2.4	2.8	0.8	0.5
7	5.6	4.3	1.2	1.4

[a]Determined using the ratio of the IC_{50} against nontumorigenic CCD1065SK HDF cells over the IC_{50} against four cancer cell lines.

Table 4. Selective Indices of 1−7[a]

compound	BT-474	MCF-7	AU565	MDA-MB-231
1	1.8	1.6	0.3	0.5
2	8.9	14	N/A	13
3	10.5	26	N/A	25
4	0.4	0.7	0.2	0.2
5	1.0	0.9	0.3	0.4
6	9.2	10.9	3.1	2.0
7	0.7	0.5	0.1	0.2

[a]Determined using the ratio of the IC_{50} against nontumorigenic sheep erythrocytes over the IC_{50} against four cancer cell lines.

Biological Activity of Surfactin and Its Synthetic Analogues in Three-Dimensional Cultures. Traditional two-dimensional (2D) breast cancer cell cultures may not adequately recapitulate the *in vivo* microenvironment and cell morphology. This is due to the lack of a three-dimensional (3D) context in which the aggregation of cancer cells changes their cell morphology, altering their cellular and extracellular interactions, and method of cell division. To this end, 3D spheroid models of both the MDA-MB-231 and BT-474 cells were prepared to better mimic the structure and pathophysiological gradients seen for *in vivo* solid tumors.[34,35] These studies focused on **1** as well as the most promising cationic, amplified anionic, and neutral synthetic surfactin drug candidates (**2**, **4**, and **7**, respectively).

We expected, based on previous studies by ourselves[36] and others,[35,37,38] and anticipated that 3D tumor cell aggregates in a spheroid morphology would lead to higher IC_{50} values. Hence, dose−response biological activity assays were extended for BT-474 (Figure 3A) and MDA-MB-231 (Figure 3B) cell lines to 3D tumor aggregates, prepared using liquid-overlay with Matrigel following previous work by our group.[36,39,40] Briefly, MDA-MB-231 or BT-474 cell lines, selected for their stark differences in morphology and cell receptor presence, were seeded in a 96-well plate in the presence of Matrigel, centrifuged to form 3D tumor spheroids, and allowed to incubate for 4 days. Following 24 h treatment of MDA-MB-231 3D spheroids, the IC_{50} value for **1** was 140 μg/mL,

https://doi.org/10.1021/acsomega.3c00454
ACS Omega 2023, 8, 14610−14620

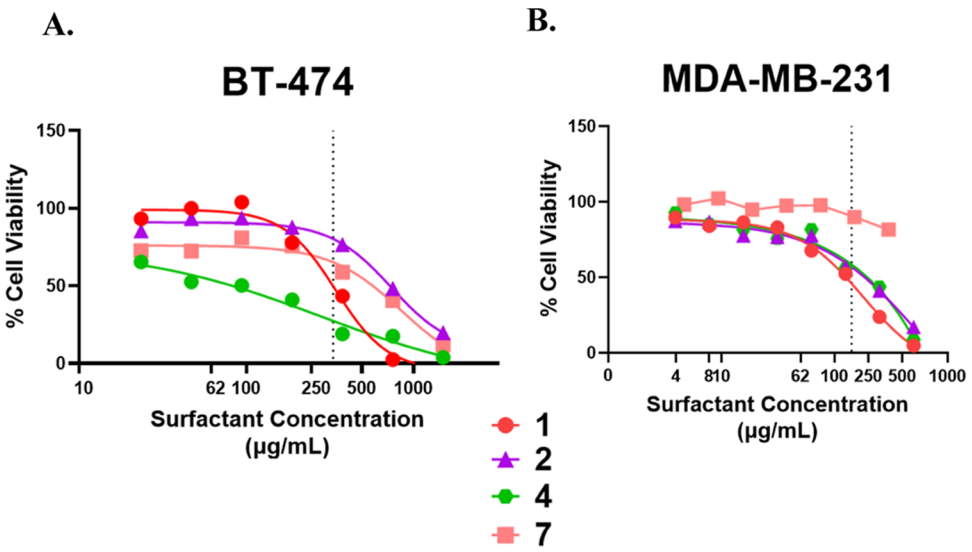

Figure 3. Liquid-overlay generated 3D spheroid IC_{50} of 1−7 after 24 h of treatment on two breast cancer cell lines: BT-474 (A) and MDA-MB-231 (B). Cell lines were selected due to their stark differences in receptor presence and morphologies. All experiments were performed in triplicate. IC_{50} determined with AbsoluteIC50 nonlinear regression curve on GraphPad9. The dotted vertical line represents the IC_{50} of **1**.

representing a 1.7-fold increase over that of 2D monolayer cultures (Table 5). The IC_{50} values of **2** and **4** were 170 and 190 μg/mL, representing a 12-fold and 9-fold increase over their respective 2D monolayer IC_{50} values, respectively. These results indicate that **1** and selected analogues have difficulty penetrating spheroids that present thicker gradients for nutrient/waste/drug transport. Compared to MDA-MB-231 cells, BT-474 cells exhibited larger increases in IC_{50} when moving from the 2D monolayer to 3D spheroid model. In BT-474 cells, **1** showed a nearly 16-fold increase in IC_{50} when moving from the 2D (21 ug/mL) to 3D (330 ug/mL) cell model. Similarly, dosing with **2** and **4** resulted in IC_{50} values > 700 μg/mL (9-fold increase) and 200 μg/mL (3-fold increase), respectively. MDA-MB-231 forms less dense aggregates than BT-474, which develops tightly packed aggregates.[41,42] Correspondingly, BT-474 cells exhibited larger IC_{50} increases when moving from 2D to 3D than MDA-MB-231 cells (Table 5). Taken together, these findings are consistent with the reduced permeability of surfactin and its analogues in the more dense BT-474 spheroid than MDA-MB-231. Future studies are necessary to investigate the mechanisms for the high recalcitrance of BT-474 spheroids to natural and synthetic surfactins as well as to identify further structural modifications or delivery vehicles that overcome this barrier to drug effectiveness.

Table 5. IC_{50} Values for Liquid-Overlay Generated 3D Spheroids of Two Cell Lines[a,b]

compound	BT-474	MDA-MB-231
1	330	140
2	760	190
4	200	170
7	730	N/A

[a]Dose−response curves seen in Figure 3 for compounds **1**, **2**, **4**, and 7. [b]Note: values represented as μg/mL, n = 3/dose.

Mechanism of Action on MDA-MB-231 and BT-474. After evaluating IC_{50} values against the four tumorigenic cell lines and two nontumorigenic lines, the most promising cationic, amplified anionic, and neutral synthetic surfactin drug candidates (see above), based on the overall activity and SI

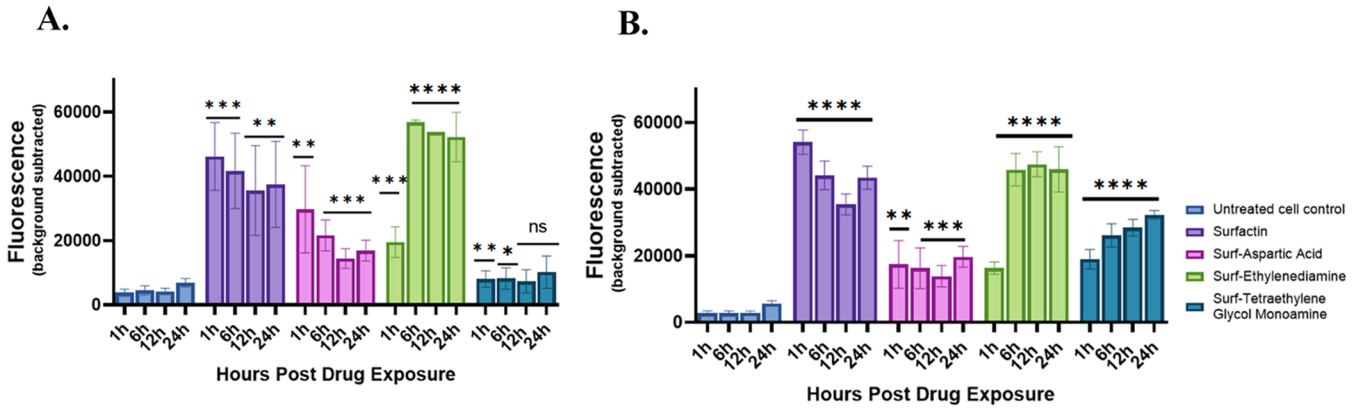

Figure 4. Measurement of cell lysis in BT-474 (A) and MDA-MB-231 (B) after 24 h of surfactin treatment. Significant increases in cell lysis occurred for every time point and compound in MDA-MB-231 and BT-474 cells, with the exception of **7** in BT-474 cells. Significance was determined with one-sample t-test, P value < 0.05, n = 6.

https://doi.org/10.1021/acsomega.3c00454
ACS Omega 2023, 8, 14610−14620

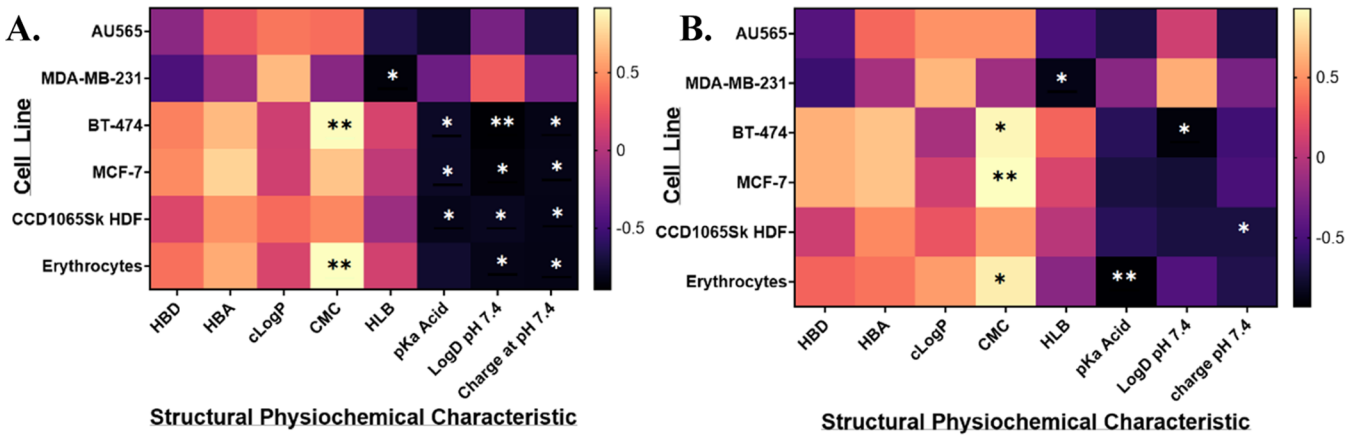

Figure 5. Correlation of biological activity and structural physicochemical characteristics. Biological activity of each cell line is given by experimentally determined IC_{50} values for individual surfactin analogues. Pearson's test (A) indicates linear significance, and Spearman's test (B) indicates the strength of nonlinear monotonic associations. Significance determined using Graphpad Prism9 Pearson's and Spearman's tests; $P < 0.05$ is denoted by *, $P < 0.01$ denoted by **.

values (see above) as well as **1**, were investigated to elucidate mechanism(s) by which they inhibit breast cancer cell growth. For **1**, previous reports on the operative mechanisms for cell killing include allergic reactions through ROS-regulated apoptosis,[43,44] disruptions to plasma membrane composition,[18] and ER-stress-mediated apoptosis.[19]

We investigated whether elevated levels of caspase-3 and caspase-7 are found in cell media post 24 h of drug exposure for BT-474 and MDA-MB-231 cell lines to determine if apoptosis was a major cause of cell death, as previously claimed by others.[45,46] Caspase-3 controls morphological changes in apoptosis and DNA fragmentation, while caspase-7 is believed to have greater importance in the loss of cellular viability.[47] Results indicated that BT-474 cell death was not caused by apoptosis, while only **3** caused a significant ($P < 0.05$) increase in caspase-3/7 in the MDA-MB-231 cells, compared with untreated control cells (Figure S17B,C). For both cell lines, the amount of caspase-3/7 detected was below that of the untreated control (Figure S17B,C). This is potentially due to the increased cell death of each cell line over the basal levels of caspase-3/7 found in untreated cells. A cell viability assay was run in tandem with the caspase-3/7 assay to confirm that at least 50% of MDA-MB-231 cells were killed by exposure to **1** and its derivatives (Figure 17SA). Although the cell viability assays confirmed that cell death was occurring in response to treatment with natural and synthetic surfactin compounds, the caspase-3/7 activity generally decreased. These results indicate that apoptosis is not the prevalent mechanism by which surfactin and its analogues affect cell growth and viability.

The extent of cell lysis that occurs for natural and synthetic surfactin compounds was determined using the CellTox green cytotoxicity assay that contains a green, fluorescent probe (Figure 4). In the absence of cell lysis, the green dye will not enter cells resulting in low or no fluorescence. At 1 h post **1** treatment, cell lysis of both BT-474 and MDA-MB-231 cells was observed. There was a significant change in the extent of cell lysis occurring 1 h after drug exposure as a function of the synthetic surfactin structure; however, there was minimal to no increase in lysis beyond 1 h of exposure. For the treatment of BT-474 and MDA-MB-231 cells with **4**, the extent of cell lysis increased from 1 to 6 h, after which no further increase in the fluorescence intensity was observed. The extent of cell lysis of both BT-474 and MDA-MB-231 was similar when exposed to **1** and **4**. Compound **7** caused low extents of BT-474 cell lysis. In contrast, **7** was more effective in lysing MDA-MB-231 cells, and the extent of cell lysis increased with exposure time. Compound **3** also induced cell lysis for both cancer cell lines though the extent of cell lysis was less than for exposures to **1** and **4**. The high extent of cell lysis indicates that a nonapoptotic pathway is initiated by drug exposure. Further investigation is necessary to confirm the cell death mechanism of action.

Structural Physicochemical Characteristics for Surfactin and Its Synthetic Analogues. Two computational approaches were used to correlate the structural physicochemical characteristics and biological activity for each cell line (Figure 5). Pearson's test for linear correlations showed a positive and significant slope (R value) between increased activity with decreased CMC for erythrocytes ($P = 0.0039$) and BT-474 ($P = 0.0052$) cells. Spearman's nonlinear test also found a significant positive correlation (R value) in CMC for BT-474, MCF-7, and erythrocytes ($P < 0.05$). However, there was no significant correlation between CMC and biological activity in the nontumorigenic cell line CCD1065SK HDF. CMC may play a key role in tumorigenic biological activity, and therefore, the modification of CMC may provide a useful opportunity for drug surfactin structural modification in future studies. Pearson's test also found a significant negative correlation (R value) between decreased activity and increased pK_a, $\log D$, and charge at pH 7.4 for BT-474, MCF-7, CCD1065SK HDF, and erythrocytes ($P < 0.05$). To the best of our knowledge, this is the first report to identify correlations between structure and activity for a series of microbial synthetic surfactants. This data will inform further modifications of **1** to further improve biological activity and selectivity.

In conclusion, we sought to chemically modify surfactin, a cyclic-lipopeptide generated by a *B. subtilis*. L-Glu and L-Asp moieties were selected for amidation reactions to alter the overall charge, size, and hydrophilicity of resulting analogues. Novel synthetic analogues **2**–**7** were generated by simple amidation reactions; two anionic, three cationic, and one neutral. The two anionic compounds, **2** and **3**, reduced activity against red blood cells and nontumorigenic fibroblasts, while cationic **4** and neutral **7** had greatly increased activity against both tumorigenic and nontumorigenic cell lines. Early insight into a mechanism of action suggests that cell lysis plays a

https://doi.org/10.1021/acsomega.3c00454
ACS Omega 2023, 8, 14610−14620

critical role, and hence, membrane permeabilization is hypothesized to be critical. However, additional studies are needed to determine whether multiple mechanisms are involved. It is critical to further reduce hemolytic activity, and a more comprehensive understanding of the differences between 2D and 3D cell models is required to transition to a more *in vivo* microenvironment.

MATERIALS AND EXPERIMENTAL METHODS

Surfactin Synthesis Materials. Sodium surfactin was purchased from Formulator Sample Shop (SKU#FSSB30098). Surfactin was column-purified under silica gel column chromatography, using 1:9 analytical grade chloroform/methanol mixtures as eluents. Purity was confirmed by NMR and ESI-MS. HATU 1-[bis(dimethylamino)methylene]-1*H*-1,2,3-trizolo[4,5-*b*]pyridinium 3-oxide hexafluorophosphate, N-BOC-ethylenediamine, L-glutamic acid di-*tert*-butyl ester hydrochloride, L-aspartic acid di-*tert*-butyl ester hydrochloride, 2-(2-aminoethyl)-1,3-di-BOC guanidine, and L-histamine were purchased from Sigma-Aldrich at the highest purity available. Tetraethylene glycol monoamine was purchased from Chem Impex at 98% purity. Cell counting kit-8 (CCK-8) was purchased from Sigma-Aldrich. Matrigel was purchased from Corning. CellTiter 3D Cell Viability Assay and the CellTox Green Cytotoxicity Assay were purchased from Promega. Sheep red blood cells (RBCs) were obtained from Innovative Research, Inc. (Novi, MI).

General Method for Molecular Engineering of Surfactin. In a 50 mL round-bottom flask, 250 mg of purified surfactin (48 mmol) and an amine-containing reactant (2.2−2.5 equiv) were dissolved in dimethylformamide (DMF) (5 mL) under magnetic stirring. Then, hexafluorophosphate azabenzotrizole tetramethyl uronium (HATU) (202 mg, 1.1 equiv), and *N*,*N*-diisopropylethylamine (DIPEA) (124 mg, 2.2 equiv) were added to the flask. The reaction was maintained at an ambient temperature with stirring for 16−24 h. Reaction completion was confirmed by thin-layer chromatography (Sigma-Aldrich, silica gel 60 matrix, 0.2 mm thickness), using analytical grade chloroform:methanol:water (65:35:4) as an eluent. Visualization of eluted spots occurred by heating treated plates with cerium−ammonium−molybdate solution. Then, the mixture was diluted with 30 mL of analytical grade dichloromethane and washed using 30 mL of each wash in a separatory funnel with 0.1 M aqueous hydrochloric acid, saturated aqueous $NaHCO_3$ solution (1 × 10 mol/L), brine (1 × 10 mol/L), and DI water. The organic layer was dried with magnesium sulfate ($MgSO_4$) and filtered, and the solvent was removed by rotoevaporation. If a protecting group was used, a 1 mL volume of 1:1 DCM:TFA was added to the resulting product and stirred at RT for 3 h. Reaction completion was confirmed by TLC. The crude product was purified by silica gel column chromatography using a 40:1 w/w ratio of silica to product and eluents consisting of analytical grade chloroform and methanol gradient elution mixtures of 9:1, 8:2, and 1:1. TLC was utilized as above to monitor the range of volumes in which the product eluted as well as its purity. The purified products were characterized by proton (^{1}H) nuclear magnetic resonance (NMR) spectra recorded in DMSO-d_6 on a Bruker spectrophotometer at 600 MHz and LC/MS spectra recorded on an electrospray ionization mass spectrophotometer in positive ionization mode. The melting point was characterized as well as surface tension, the latter using the Wilhemy vertical plate technique with a Krüss tensiometer (Mathews, NC). Variations in the above synthetic method required for specific surfactin analogues are described in the Supporting Information section along with product appearance, melting point, ^{1}H NMR, inverse-gated decoupling ^{13}C-NMR, and LC-MS results (Figures S1−S15).

Cell Culture Materials. CCD1065Sk human dermal fibroblasts (HDFs) (ATCC, Manassas, VA), derived from mammary epithelial tissue, were grown in standard cell culture conditions (37 °C, 5% CO_2, 95% RH) in Dulbecco's modified Eagle's medium (DMEM) supplemented with 15% (v/v) fetal bovine serum (FBS) and 0.5% (v/v) penicillin/streptomycin. MCF-7 human breast epithelial adenocarcinoma cells (ATCC, Manassas, VA), MDA-MB-231 triple negative human breast adenocarcinoma cells, and BT-474 human breast ductal carcinoma cells (ATCC, Manassas, VA) were grown in standard cell culture conditions (37 °C, 5% CO_2, 95% RH) in DMEM without phenol red, supplemented with 10% (v/v) FBS. AU565 human breast adenocarcinoma cells (ATCC, Manassas, VA) were grown in standard cell culture conditions (37 °C, 5% CO_2, 95% RH) in Roswell Park Memorial Institute (RPMI)-1640 growth medium supplemented with 10% (v/v) fetal bovine serum (FBS), 100 U/mL of penicillin/streptomycin, and 2 mM L-glutamine.

2D Dose−Response Assay. To prepare 2D monolayer cultures, cells were trypsinized, centrifuged, and resuspended in media at 250,000 cells/mL. A 100 μL of cell suspension was added to each well of a 96-well flat-bottom well plate and cells were cultured for 24 h prior to compound testing. Compounds were individually solubilized in 100% DMSO, followed by dilutions to concentrations from 5000 to 40 μg/mL in 1:2 serial dilutions in fresh media; 10 μL of each corresponding drug concentration was added to each well in triplicate—thus, each concentration has been diluted 10-fold due to the 100 μL of media present in the well from cell seeding. Care was taken such that the final concentration of DMSO was no more than 1% per well. Wells consisting of media without cells and untreated cells served as a positive and negative control, respectively. After drug addition, cells were placed in a cell culture incubator (5% CO_2, 37 °C) for 24 h, and cell viability was assessed by a Cell Counting Kit-8 (CCK-8) assay, following the manufacturer's protocol[48] and using a BioTek μQuant Microplate Reader (BioTek Instruments). Half-maximal inhibitory concentration (IC_{50}) was calculated with the use of GraphPad Prism9 software, absolute IC_{50} determination.

3D Dose−Response Assay. Utilizing previously published methods,[27] a liquid-overlay technique was utilized for the formation of tumor aggregates. Cells were trypsinized, centrifuged, and resuspended in media at 250,000 cells/mL. The cell suspension (100 μL) was added to each well of a round-bottom, nonadherent, 96-well plate (CellStar, Greiner Bio-One). Matrigel (2.5% v/v) was added to each well, and, immediately after, the plate was centrifuged for 10 min at 1000 rpm to ensure collection of a cell pellet at the bottom of each well. Plates were incubated, and cell aggregates were cultured over a 4 day maturation period prior to compound testing.[36,39,40] Compounds were individually solubilized in 100% DMSO, followed by dilutions to concentrations from 10,000 to 80 μg/mL in 1:2 serial dilutions; 10 μL of each corresponding drug concentration was added to each well in triplicate—thus, each concentration has been diluted 10-fold due to the 100 μL of media present in the cell from cell seeding. Care was taken such that the final concentration of

https://doi.org/10.1021/acsomega.3c00454
ACS Omega 2023, 8, 14610−14620

DMSO was no more than 1% v/v per well. Wells consisting of media without cells and untreated cells served as a positive and negative control, respectively. After drug addition, cells were placed in a cell culture incubator (5% CO_2, 37 °C) for 24 h, and cell viability was assessed by a CellTiter 3D Cell Viability Assay following the manufacturer's protocol[49] and using a Tecan Infinite M1000 PRO Multi-Well Plate Reader. Half-maximal inhibitory concentration (IC_{50}) was calculated with the use of GraphPad Prism9 software, absolute IC_{50} determination.

Critical Micelle Concentration. Surface tensions of modified surfactin compounds were measured with a Kruss K100 Tensiometer using a Wilhelmy platinum plate as a probe. Samples were freshly prepared in a clean, dry 50 mL beaker at 22 °C, using a 0.1 M solution of $NaHCO_3$ at pH 8.7. All measurements were carried out in triplicate. Linear regression of drop and flat areas was performed separately for the surface tension concentration curve. The concentration at the intersection of two lines is the CMC.

Hemolytic Activity. Fresh sheep blood cells (RBCs) were used to determine IC_{50}, defined as the concentration at which 50% of the RBCs are lysed. RBCs were first washed with PBS (pH 7.4) until the supernatant was visually clear, after which they were centrifuged at 1000 rpm for 8 min. Clean RBCs (2% v/v) were treated with surfactin derivatives in PBS containing 5% DMSO at predetermined concentrations ranging from 2000 to 5 μg/mL These mixtures were then incubated at 37 °C for 1 h. The RBCs were centrifuged at 1000 rpm for 8 min at room temperature; 200 μL of the supernatant was transferred to a 96-well plate and, using a BioTek uQuant Microplate Reader (BioTek Instruments), absorbance at 540 nm and background absorbance at 630 nm were recorded. PBS (pH 7.4) containing DMSO (5% v/v) served as the negative control, whereas RBC (2% v/v) in PBS containing DMSO (5% v/v) treated with 1% v/v Triton X-100 was a positive control. Measurements were completed in triplicate.

Structural Physicochemical Characteristic Determination. SMILES notation of compounds **1**−**7** was used to generate all physicochemical characterizations, except for CMC, using Chemicalize software. Furthermore, using GraphPad Prism9, each physicochemical characteristic was plotted against each individual cell line for compounds **1**−**7** to determine Pearson's linear correlation and Spearman's nonlinear correlation analysis. R^2 and P values were reported for each output. The R^2 value was shown in a heatmap format, with a significance of $P < 0.05$ denoted as * and $P < 0.01$ denoted as ** for each test.

Caspase-Glo 3/7 Assay for Apoptosis Detection. Insight into an apoptotic mechanism was explored with the use of the caspase-Glo 3/7 assay system (Promega, Cat#G8091). Separate 2D monolayers of MDA-MB-231 and BT-474 cells were seeded at 200,000 cells/mL (100 μL per well) in a white, flat-bottom 96-well plate and placed in a cell culture incubator overnight to allow cell adherence. Cells were drugged with either **1**, **2**, **4**, or **7** at their respective IC_{50} values. Diluted concentrations were prepared by using a stock solution of each compound in 100% DMSO, which was diluted in fresh media until a concentration 10-fold higher than that to be used in assays was attained. Then, 10 μL of each compound was added to each well, which resulted in the final 10× dilution such that the compound concentration is equivalent to the IC_{50} dose. After drug exposure, cells were placed in a cell culture incubator (5% CO_2, 37 °C) for 24 h to allow cell death to occur. Following the manufacturer's protocol,[50] the wells were seeded and drugged to their respective IC_{50} values; incubations at 37 °C were continued for 24 h, and, thereafter, the plate was maintained at room temperature for 30 min. Then, 100 μL of the caspase-3/7 reagent was added to each well containing cells. The plate was then placed on a plate shaker at 400 RPM for 30 s at RT. Immediately following the plate shake, the plate was allowed to sit at RT for 2 h to allow for luciferase stabilization. A Tecan Infinite M1000 PRO Multi-Well Plate Reader, in scanning luminescence mode, measured the luminescence from each well. Assays were completed in triplicate. Significance was determined by GraphPad Prism9 using a one-sample t-test against the mean of the untreated control at each respective hour post drug exposure. Significance shown as $P < 0.05$ denoted as *, $P < 0.01$ as **, $P < 0.001$ as ***, and $P < 0.0001$ as ****.

CellTox Green Cytotoxicity Assay: Cell Lysis. Cell lysis-based cell death was investigated by the CellTox Green Cytotoxicity Assay from Promega. Separate 2D monolayers of MDA-MB-231 and BT-474 cells were seeded at 200,000 cells/mL (100 μL per well) in a black, flat 96-well plate. Cells were placed in a cell culture incubator overnight to allow for cell adherence. Cells were drugged with either **1**, **2**, **4**, or **7** at their respective IC_{50} values. Concentration dilutions were completed using a stock solution of each compound in 100% DMSO, which were further diluted in fresh media to the 10× desired concentration (10 μL of each compound was added to each well, thus accounting for the 10× dilution factor to complete the desired IC_{50} dose). Per the manufacturer's instructions,[51] 10 μL of the CellTox Green Dye that functioned as the cell lysis detection agent was added to each well immediately following the addition of each respective drug. Thereafter, the express no-step addition at dosing method was utilized according to the manufacturer's protocol.[51] Fluorescence was recorded at 485ex/510em wavelengths using a Tecan Infinite M1000 PRO Multi-Well Plate Reader at RT in fluorescence intensity mode at 1, 6, 12, and 24 h post drug exposure. Significance was determined by GraphPad Prism9 using a one-sample *t*-test against the mean of the untreated control at each respective hour post drug exposure. Significance shown as $P < 0.05$ denoted as *, $P < 0.01$ as **, $P < 0.001$ as ***, and $P < 0.0001$ as ****.

■ ASSOCIATED CONTENT

Supporting Information

The Supporting Information is available free of charge at https://pubs.acs.org/doi/10.1021/acsomega.3c00454.

NMR spectra and LC-MS spectra for all compounds and additional experimental details and methods (PDF); surface tension measurements and caspase-3/7 plots (PDF)

■ AUTHOR INFORMATION

Corresponding Author

Richard A. Gross − *Center for Biotechnology and Interdisciplinary Sciences and Department of Chemistry and Chemical Biology, Rensselaer Polytechnic Institute, Troy, New York 12180, United States;* orcid.org/0000-0002-5050-3162; Phone: (518) 577-1090; Email: grossr@rpi.edu

https://doi.org/10.1021/acsomega.3c00454
ACS Omega 2023, 8, 14610−14620

Authors

Rebecca T. Miceli − *Center for Biotechnology and Interdisciplinary Sciences, Department of Chemistry and Chemical Biology, and Department of Biomedical Engineering, Rensselaer Polytechnic Institute, Troy, New York 12180, United States;* orcid.org/0000-0002-2297-9219

Filbert Totsingan − *Department of Chemistry and Chemical Biology, Rensselaer Polytechnic Institute, Troy, New York 12180, United States*

Tasnim Naina − *Department of Chemistry and Chemical Biology, Rensselaer Polytechnic Institute, Troy, New York 12180, United States*

Samita Islam − *Department of Chemistry and Chemical Biology, Rensselaer Polytechnic Institute, Troy, New York 12180, United States*

Jonathan S. Dordick − *Center for Biotechnology and Interdisciplinary Sciences, Department of Biomedical Engineering, and Department of Chemical and Biological Engineering, Rensselaer Polytechnic Institute, Troy, New York 12180, United States;* orcid.org/0000-0001-7802-3702

David T. Corr − *Department of Biomedical Engineering, Rensselaer Polytechnic Institute, Troy, New York 12180, United States*

Complete contact information is available at: https://pubs.acs.org/10.1021/acsomega.3c00454

Notes

The authors declare no competing financial interest.

■ ACKNOWLEDGMENTS

The authors would like to acknowledge Cassandra Roberge for her efforts in providing AU565 cells for dose−response assays and in the confirmation of 3D spheroid morphology of BT-474 cells using optical coherence tomography and Dr. Dmitri Zagorevski for his help in producing the LC-MS protocol for compounds **1**−**7**. This work was supported by the National Institutes of Health (NIH) R01 CA233188 (DTC), NIGMS T32GM067545 (RTM), NSF PFI Award #2141034 (RAG), and the Warren Alpert Foundation (JSD).

■ REFERENCES

(1) Zhao, H.; Shao, D.; Jiang, C.; Shi, J.; Li, Q.; Huang, Q.; Rajoka, M. S. R.; Yang, H.; Jin, M. Biological Activity of Lipopeptides from Bacillus. *Appl. Microbiol. Biotechnol.* **2017**, *101*, 5951−5960.

(2) Thanomsub, B.; Pumeechockchai, W.; Limtrakul, A. Chemical Structures and Biological Activities of Rhamnolipids Produced by Pseudomonas Aeruginosa B189 Isolated from Milk Factory Waste. *Bioresour. Technol.* **2006**, *97*, 2457−2461.

(3) Otzen, D. E. Biosurfactants and Surfactants Interacting with Membranes and Proteins: Same but Different? *Biochim. Biophys. Acta, Biomembr.* **2017**, *1859*, 639−649.

(4) Zhao, H.; Zhao, X.; Lei, S.; Zhang, Y.; Shao, D.; Jiang, C.; Sun, H.; Shi, J. Effect of Cell Culture Models on the Evaluation of Anticancer Activity and Mechanism Analysis of the Potential Bioactive Compound, Iturin A, Produced by: Bacillus Subtilis. *Food Funct.* **2019**, *10*, 1478−1489.

(5) Santos, D. K. F.; Rufino, R. D.; Luna, J. M.; Santos, V. A.; Sarubbo, L. A. Biosurfactants: Multifunctional Biomolecules of the 21st Century. *Int. J. Mol. Sci.* **2016**, *17*, No. 401.

(6) Dierickx, S.; Castelein, M.; Remmery, J.; De Clercq, V.; Lodens, S.; Baccile, N.; De Maeseneire, S. L.; Roelants, S. L. K. W.; Soetaert, W. K. From Bumblebee to Bioeconomy: Recent Developments and Perspectives for Sophorolipid Biosynthesis. *Biotechnol. Adv.* **2021**, *54*, No. 107788.

(7) Willenbacher, J.; Zwick, M.; Mohr, T.; Schmid, F.; Syldatk, C. Evaluation of Different Bacillus Strains in Respect of Their Ability to Produce Surfactin in a Model Fermentation Process with Integrated Foam Fractionation. *Appl. Microbiol. Biotechnol.* **2014**, 9623−9632.

(8) Chen, H. L.; Chen, Y. S.; Juang, R. S. Flux Decline and Membrane Cleaning in Cross-Flow Ultrafiltration of Treated Fermentation Broths for Surfactin Recovery. *Sep. Purif. Technol.* **2008**, *62*, 47−55.

(9) Willenbacher, J.; Yeremchuk, W.; Mohr, T.; Syldatk, C.; Hausmann, R. Enhancement of Surfactin Yield by Improving the Medium Composition and Fermentation Process. *AMB Express* **2015**, *5*, No. 57.

(10) Klausmann, P.; Hennemann, K.; Hoffmann, M.; Treinen, C.; Aschern, M.; Lilge, L.; Morabbi Heravi, K.; Henkel, M.; Hausmann, R. Bacillus Subtilis High Cell Density Fermentation Using a Sporulation-Deficient Strain for the Production of Surfactin. *Appl. Microbiol. Biotechnol.* **2021**, *105*, 4141−4151.

(11) De Faria, A. F.; Teodoro-Martinez, D. S.; De Oliveira Barbosa, G. N.; Gontijo Vaz, B.; Serrano Silva, Í.; Garcia, J. S.; Tótola, M. R.; Eberlin, M. N.; Grossman, M.; Alves, O. L.; Regina Durrant, L. Production and Structural Characterization of Surfactin (C 14/Leu7) Produced by Bacillus Subtilis Isolate LSFM-05 Grown on Raw Glycerol from the Biodiesel Industry. *Process Biochem.* **2011**, *46*, 1951−1957.

(12) Shaligram, N. S.; Singhal, R. S. Surfactin -a Review on Biosynthesis, Fermentation, Purification and Applications. *Food Technol. Biotechnol.* **2010**, *48*, 119−134.

(13) da Costa Vieira, R. A.; Biller, G.; Uemura, G.; Ruiz, C. A.; Curado, M. P. Breast Cancer Screening in Developing Countries. *Clinics* **2017**, *72*, 244−253.

(14) Jeong, Y.-J.; Kang, J. S.; Lee, S. I.; So, D. M.; Yun, J.; Baek, J. Y.; Kim, S. K.; Lee, K.; Park, S.-K. Breast Cancer Cells Evade Paclitaxel-Induced Cell Death by Developing Resistance to Dasatinib. *Oncol. Lett.* **2016**, *12*, 2153−2158.

(15) Hajare, S. N.; Subramanian, M.; Gautam, S.; Sharma, A. Biochimie Induction of Apoptosis in Human Cancer Cells by a Bacillus Lipopeptide Bacillomycin D. *Biochimie* **2013**, *95*, 1722−1731.

(16) Cao, X.; Jiao, Æ. A. H. W. Æ. R. Z.; Mao, C. L. W. Æ. D. Z.; Zeng, Æ. L. Y. Æ. B.; Ao, A. Á. A. Á. Surfactin Induces Apoptosis and G 2 / M Arrest in Human Breast Cancer MCF-7 Cells Through Cell Cycle Factor Regulation. *Cell Biochem. Biophys.* **2009**, *55*, 163−171.

(17) Park, S. Y.; Kim, J. H.; Lee, Y. J.; Lee, S. J.; Kim, Y. Surfactin Suppresses TPA-Induced Breast Cancer Cell Invasion through the Inhibition of MMP-9 Expression. *Int. J. Oncol.* **2013**, *42*, 287−296.

(18) Wójtowicz, K.; Czogalla, A.; Trombik, T.; Łukaszewicz, M. Surfactin Cyclic Lipopeptides Change the Plasma Membrane Composition and Lateral Organization in Mammalian Cells. *Biochim. Biophys. Acta, Biomembr.* **2021**, *1863*, No. 183730.

(19) Wang, G. S.; Chen, J. Y.; Chen, W. C.; Wei, I. C.; Lin, S. W.; Liao, K. W.; Yang, T. S.; Liu, J. F. Surfactin Induces ER Stress-Mediated Apoptosis via IRE1-ASK1-JNK Signaling in Human Osteosarcoma. *Environ. Toxicol.* **2022**, *37*, 574−584.

(20) Liu, X.; Tao, X.; Zou, A.; Yang, S.; Zhang, L.; Mu, B. Effect of Themicrobial Lipopeptide on Tumor Cell Lines: Apoptosis Induced by Disturbing the Fatty Acid Composition of Cell Membrane. *Protein Cell* **2010**, *1*, 584−594.

(21) Kracht, M.; Rokos, H.; Özel, M.; Kowall, M.; Pauli, G.; Vater, J. Antiviral and Hemolytic Activities of Surfactin Isoforms and Their Methyl Ester Derivatives. *J. Antibiot.* **1999**, *52*, 613−619.

(22) Liu, X. Y.; Yang, S. Z.; Mu, B. Z. Production and Characterization of a C15-Surfactin-O-Methyl Ester by a Lipopeptide Producing Strain Bacillus Subtilis HSO121. *Process Biochem.* **2009**, *44*, 1144−1151.

(23) Nozhat, Z.; Asadi, A.; Zahri, S. Properties of Surfactin C-15 Nanopeptide and Its Cytotoxic Effect on Human Cervix Cancer (HeLa) Cell Line. *J. Nanomater.* **2012**, *2012*, 1−5.

(24) Yuan, L.; Zhang, S.; Peng, J.; Li, Y.; Yang, Q. Synthetic Surfactin Analogues Have Improved Anti-PEDV Properties. *PLoS One* **2019**, *14*, No. e0215227.

(25) Hirschhaeuser, F.; Menne, C.; Dittfeld, J.; West, W.; Muller-Klieser, W.; Kunz-Schughart, L. A. Multicellular Tumor Spheroids: An Underestimated Tool Is Catching up Again. *J. Biotechnol.* **2010**, *148*, 3−15.
(26) Mueller-Klieser, W. Multicellular Spheroids: A Review on Cellular Aggregates in Cancer Research. *J. Cancer Res Clin Oncol.* **1987**, *113*, 101−122.
(27) Nagelkerke, A.; Bussink, J.; Sweep, F. C. G. J.; Span, P. N. Generation of Multicellular Tumor Spheroids of Breast Cancer Cells: How to Go Three-Dimensional. *Anal. Biochem.* **2013**, *437*, 17−19.
(28) Lipinski, C. A.; Lombardo, F.; Dominy, B. W.; Feeney, P. J. Experimental and Computational Approaches to Estimate Solubility and Permeability in Drug Discovery and Development Settings. *Adv. Drug Delivery Rev.* **2012**, *64*, 4−17.
(29) Ishibashi, Y.; Osman, M.; Nakahara, H.; Sano, Y.; Ishiguaro, R.; Matsumoto, M. Significance of B-Sheet Formation for Micellization and Surface Adsorption of Surfactin. *Colloids Surf., A* **1994**, *4*, 341−348.
(30) Dai, X.; Cheng, H.; Bai, Z.; Li, J. Breast Cancer Cell Line Classification and Its Relevance with Breast Tumor Subtyping. *J. Cancer* **2017**, *8*, 3131−3141.
(31) Fei, D.; Liu, F.; Gang, H.; Liu, J.; Yang, S.; Ye, R.; Mu, B. A New Member of the Surfactin Family Produced by Bacillus Subtilis with Low Toxicity on Erythrocyte. *Process Biochem.* **2020**, *94*, 164−171.
(32) Colonnna, W. J.; Marti, M. E.; Nyman, J. A.; Green, C.; Glatz, C. E. Hemolysis as a Rapid Screening Technique for Assessing the Toxicity of Native Surfactin and a Genetically Engineered Derivative. *Environ. Prog. Sustainable Energy* **2016**, *36*, 505−510.
(33) Lica, J. J.; Wieczór, M.; Grabe, G. J.; Heldt, M.; Jancz, M.; Misiak, M.; Gucwa, K.; Brankiewicz, W.; Maciejewska, N.; Stupak, A.; Bagiński, M.; Rolka, K.; Hellmann, A.; Składanowski, A. Effective Drug Concentration and Selectivity Depends on Fraction of Primitive Cells. *Int. J. Mol. Sci.* **2021**, *22*, No. 4931.
(34) Kessel, S.; Cribbes, S.; Déry, O.; Kuksin, D.; Sincoff, E.; Qiu, J.; Chan, L. L. Y. High-Throughput 3D Tumor Spheroid Screening Method for Cancer Drug Discovery Using Celigo Image Cytometry. *SLAS Technol.* **2017**, *22*, 454−465.
(35) Friedrich, J.; Seidel, C.; Ebner, R.; Kunz-Schughart, L. A. Spheroid-Based Drug Screen: Considerations and Practical Approach. *Nat. Protoc.* **2009**, *4*, 309−324.
(36) Roberge, C. L.; Miceli, R. T.; Murphy, L. R.; Kingsley, D. M.; Gross, R. A.; Corr, D. T.Sophorolipid Candidates Demonstrate Cytotoxic Efficacy Against 2D And 3D Breast Cancer Models *bioRxiv Prepr.* 2022 DOI: 10.1101/2022.09.01.506226.
(37) Langhans, S. A. Three-Dimensional in Vitro Cell Culture Models in Drug Discovery and Drug Repositioning. *Front. Pharmacol.* **2018**, *9*, No. 6.
(38) Huang, Z.; Yu, P.; Tang, J. Characterization of Triple-Negative Breast Cancer MDA-MB-231 Cell Spheroid Model. *OncoTargets Ther.* **2020**, *13*, 5395−5405.
(39) Roberge, C. L.; Kingsley, D. M.; Faulkner, D. E.; Sloat, C. J.; Wang, L.; Barroso, M.; Intes, X.; Corr, D. T. Non-Destructive Tumor Aggregate Morphology and Viability Quantification at Cellular Resolution, During Development and in Response to Drug. *Acta Biomater.* **2020**, *117*, 322−334.
(40) Roberge, C. L.; Wang, L.; Barroso, M.; Corr, D.Non-Destructive Evaluation of Regional Cell Density Within Tumor Aggregates Following Drug Treatment *J. Vis. Exp.* 2022 DOI: 10.3791/64030-v.
(41) Ivascu, A.; Kubbies, M. Diversity of Cell-Mediated Adhesions in Breast Cancer Spheroids. *Int. J. Oncol.* **2007**, *31*, 1403−1413.
(42) Kim, H. Y.; Jung, H.; Kim, H. M.; Jeong, H. J. Surfactin Exerts an Anti-Cancer Effect through Inducing Allergic Reactions in Melanoma Skin Cancer. *Int. Immunopharmacol.* **2021**, *99*, No. 107934.
(43) Thuy, T.; Vo, T.; Liu, J.; Wu, C.; Lin, W.; Chen, Y.; Lee, I. Surfactin from Bacillus Subtilis Induces Apoptosis in Human Oral Squamous Cell Carcinoma through ROS-Regulated Mitochondrial Pathway. *J. Cancer* **2020**, *11*, 7253−7263.
(44) Cao, X. H.; Zhao, S. S.; Liu, D. Y.; Wang, Z.; Niu, L. L.; Hou, L. H.; Wang, C. L. ROS-Ca2+ Is Associated with Mitochondria Permeability Transition Pore Involved in Surfactin-Induced MCF-7 Cells Apoptosis. *Chem.-Biol. Interact.* **2011**, *190*, 16−27.
(45) Vo, T. T. T.; Liu, J. F.; Wu, C. Z.; Lin, W. N.; Chen, Y. L.; I-Ta, L. Surfactin from Bacillus Subtilis Induces Apoptosis in Human Oral Squamous Cell Carcinoma through ROS-Regulated Mitochondrial Pathway. *J. Cancer* **2020**, *11*, 7253−7263.
(46) Wu, Y. S.; Ngai, S. C.; Goh, B. H.; Chan, K. G.; Lee, L. H.; Chuah, L. H. Anticancer Activities of Surfactin Potential Application of Nanotechnology Assisted Surfactin Delivery. *Front. Pharmacol.* **2017**, *8*, 1−22.
(47) Brentnall, M.; Rodriguez-Menocal, L.; De Guevara, R. L.; Cepero, E.; Boise, L. H. Caspase-9, Caspase-3 and Caspase-7 Have Distinct Roles during Intrinsic Apoptosis. *BMC Cell Biol.* **2013**, *14*, No. 32.
(48) Co LLC, S.-A.. Cell Counting Kit WST- 8 *Prod. Inf. sheet* 2018; Vol. *8*, p 7.
(49) Promega. *CellTiter-Glo Luminescent Cell Viability Assay Cell Viability Assay* 2002, pp 8−10.
(50) Promega. Caspase-Glo 3/7 Assay. *Tech. Bull.* 2015.
(51) Promega. *CellTox Green Cytotoxicity Assay - Technical Manual* 2015, pp 1−22.

https://doi.org/10.1021/acsomega.3c00454
ACS Omega 2023, 8, 14610−14620